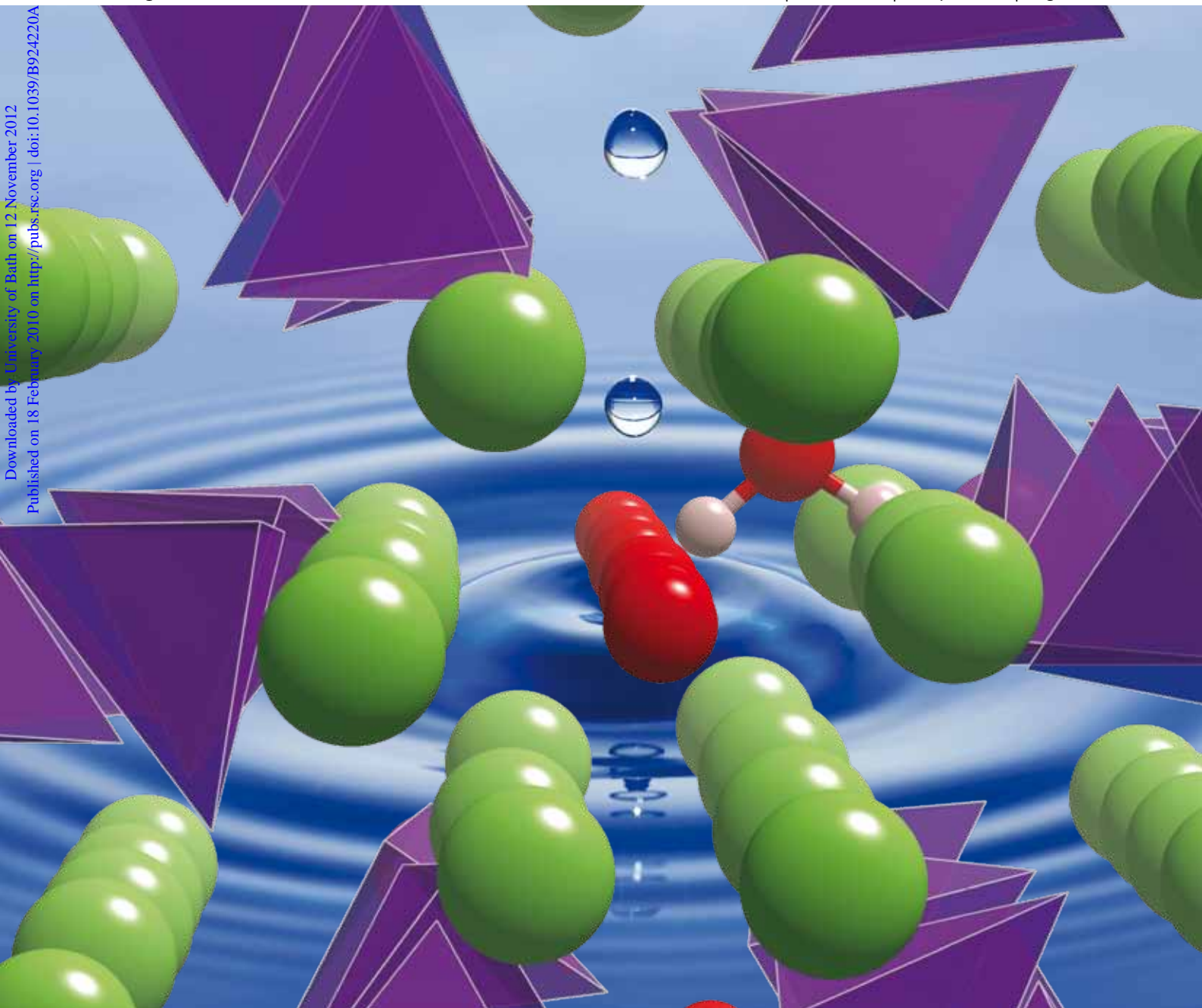


Journal of Materials Chemistry

www.rsc.org/materials

Volume 20 | Number 14 | 14 April 2010 | Pages 2693–2896



Downloaded by University of Bath on 12 November 2012
Published on 18 February 2010 on http://pubs.rsc.org | doi:10.1039/B924220A

ISSN 0959-9428

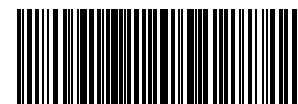
RSC Publishing

ARTICLE

M. S. Islam *et al.*
Protonic defects and water incorporation in Si and Ge-based apatite ionic conductors

20TH ANNIVERSARY ARTICLE

Peter Day *et al.*
Chiral conducting BEDT-TTF salts containing a single tris(oxalato) chromate(III) enantiomer crystallised from a chiral solvent



0959-9428(2010)20:14;1-Q

Protonic defects and water incorporation in Si and Ge-based apatite ionic conductors

P. M. Panchmatia,^a A. Orera,^b E. Kendrick,^c J. V. Hanna,^d M. E. Smith,^d P. R. Slater^b and M. S. Islam^{*a}

Received 18th November 2009, Accepted 12th January 2010

First published as an Advance Article on the web 18th February 2010

DOI: 10.1039/b924220a

Apatite-type oxide-ion conductors have attracted considerable interest as potential fuel cell electrolytes. Atomistic modelling techniques have been used to investigate oxygen interstitial sites, protonic defects and water incorporation in three silicate and three germanate-based apatite-systems, namely $\text{La}_8\text{Ba}_2(\text{SiO}_4)_6\text{O}_2$, $\text{La}_{9.33}(\text{SiO}_4)_6\text{O}_2$, $\text{La}_{9.67}(\text{SiO}_4)_6\text{O}_{2.5}$, $\text{La}_8\text{Ba}_2(\text{GeO}_4)_6\text{O}_2$, $\text{La}_{9.33}(\text{GeO}_4)_6\text{O}_2$, and $\text{La}_{9.67}(\text{GeO}_4)_6\text{O}_{2.5}$. The simulation models reproduce the complex experimental structures for all of these systems. The interstitial defect simulations have examined the lowest energy configuration and confirm this site to be near the Si/GeO₄ tetrahedra. The water incorporation calculations identify the O–H protonic site to be along the O4 oxygen channel as seen in naturally occurring hydroxy-apatites. The results also show more favourable and exothermic water incorporation energies for the germanate-based apatites. This is consistent with recent experimental work, which shows that Ge-apatites take up water more readily than the silicate analogues.

1 Introduction

Apatite materials have attracted considerable attention for a range of applications, including electrolytes for solid oxide fuel cells (SOFC), bio-ceramics for bone implants, and hazardous waste encapsulation materials. SOFC devices are of particular interest for clean energy conversion due to their high efficiency and ability to act as a bridge between hydrocarbon and hydrogen rich fuel systems.^{1–4} Yttrium-stabilized zirconia (YSZ), the current conventional electrolyte, achieves sufficient oxygen ion conductivity only at very high temperatures (1000 °C), which causes problems in terms of cell sealing, and chemical compatibility between components. For this reason, there is a substantial drive for alternative candidates operating at intermediate temperatures (500–700 °C).

A variety of material types have been considered, but this area has been dominated by the fluorite-type oxides (such as Gd/CeO₂) and perovskite oxides (such as doped LaGaO₃, BaCeO₃ and BaZrO₃). Recently, however, a range of rare-earth apatite materials have been reported as potential solid electrolyte materials, following the discovery of fast oxide ion conductivity in silicate/germanate-based systems.^{5–28} Apatite oxides have the general formula $\text{M}_{10-x}(\text{XO}_4)_6\text{O}_{2\pm y}$, where M is a rare-earth metal, such as La or an alkaline earth metal, such as Ba or Sr, and X is a p-block element such as P, Si or Ge. The structure can be described as a complex arrangement of isolated “corner sharing” XO₄ tetrahedra positioned so as to form distinct oxide ion and La channels running parallel to the *c*-axis, illustrated in Fig. 1.

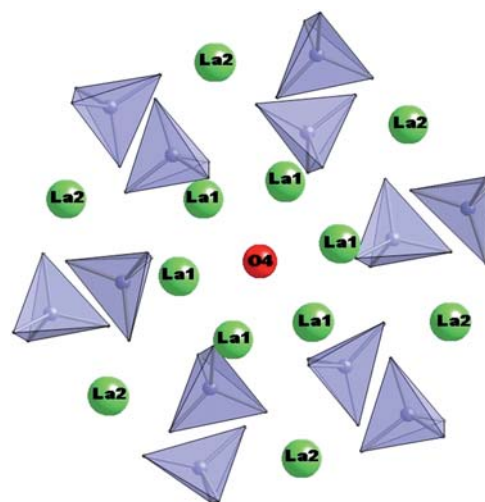


Fig. 1 Apatite oxide structure viewed down [001] showing the MO₄ tetrahedra, the La2 channels and the La1/O4 channels.

A number of rare-earth apatites have been studied for their ionic conductivity both experimentally and computationally,^{5–28} particularly focusing on the silicate and germanate analogues, in an attempt to better understand the defect chemistry driving the fast oxide-ion conductivity. Detailed dopant studies have revealed that these materials are tolerant to an unusually broad range of dopant ions, particularly on the rare-earth sites, with the observed conductivity being very sensitive to the doping and cation-anion non-stoichiometry.^{10,12,13} The highest conductivities in these apatite materials to date, have always been found for the oxygen-excess samples, indicating that the oxygen interstitials play a key role in the conduction mechanism.

Extensive modelling work on the oxygen interstitial defects and the migration pathways have been reported on stoichiometric and cation deficient systems^{9,14} and more recently on the

^aDepartment of Chemistry, University of Bath, Bath, U.K BA2 7AY. E-mail: m.s.islam@bath.ac.uk

^bSchool of Chemistry, University of Birmingham, Birmingham, U.K B15 2TT

^cChemical Sciences, University of Surrey, Guildford, Surrey, U.K GU2 7XH

^dDepartment of Physics, University of Warwick, Coventry, U.K CV4 7AL

oxygen excess silicate system.¹⁵ Nevertheless, the location of the interstitial oxide sites, and their conduction pathway have proved somewhat controversial, particular for these silicate systems. Computer modelling studies identified the presence of a favourable interstitial oxide ion site neighbouring the SiO₄ units, with subsequent experimental support from neutron diffraction, solid state NMR and Raman spectroscopy experiments.^{12,13,16} However, there have been reports of other sites closer to the oxide channel centre,^{19,20} which may indicate some dependence of the exact location of the interstitial site on sample composition or synthesis conditions.

The situation for the germanate apatites appears more consistent, with observations from both modelling and neutron diffraction studies indicating that the interstitial oxide ion is more closely associated with the GeO₄ units leading to the effective creation of five coordinate Ge.^{14,27,28}

The complexity of these apatite systems has been further highlighted by recent work on oxide ion conducting apatite-type silicates/germanates showing incorporation of significant levels of water. As a result, an enhanced conductivity in these water-enriched samples of La_{10-x}(GeO₄)₆O_{3-1.5x} has been observed by León-Reina *et al.*²² attributing this increase to proton conductivity, and suggesting that these materials are possible mixed oxide-ion and proton conductors. This feature is not unusual and has been shown previously in perovskite oxide materials²⁹⁻³² (*e.g.* doped BaCeO₃, Ba₂In₂O₅ materials), and cuspidines.³³

Orera *et al.*²⁶ have also recently investigated a range of germanate- and silicate-based systems, analysing the ability of these materials to incorporate water; they reported X-ray diffraction and thermogravimetric studies and found that the germanate-based apatites take up more water than the silicate analogues.²⁶ It is suggested in this study that water incorporation leads not only to the introduction of protonic defects (present as hydroxyl anions) but also extra interstitial oxide ions. In addition, in some cases a change in symmetry (triclinic to hexagonal) was observed on water incorporation. Both these features may be expected to result in an increase in oxide ion conductivity. Consequently the authors suggested that the conductivity enhancement may be due to an enhancement in oxide ion conductivity.²⁶

To complement and extend these recent experimental studies, we report detailed atomistic simulation studies of oxygen interstitial defects, favourable hydroxyl positions and water incorporation mechanisms. These simulation methods are now well established techniques and have been applied to a wide range of materials including defects in apatites^{9,14,15} and protons in perovskites.³² Six representative compositions were selected in total to allow us to examine the effects of cation vacancies and oxygen excess on such water incorporation; these systems are two stoichiometric (La₈Ba₂(Si/GeO₄)₆O₂), two cation deficient (La_{9.33}(Si/GeO₄)₆O₂) and two oxygen excess (La_{9.67}(Si/GeO₄)₆O_{2.5}) materials.

2 Methods

In this study, well established atomistic modelling methods embodied in the GULP code³⁴ have been used. Only a brief description is given here, as these methods have been reviewed elsewhere,^{35,36} and have been applied successfully to previous studies of other silicate or zeolite materials.^{36,37} The calculations

Table 1 (a) Interatomic potential and (b) shell model parameters for the Si/Ge-based apatite systems

(a) Interaction	<i>A</i> /eV	$\rho/\text{\AA}$	<i>C</i> /eV \AA^6
La...O	4579.2300	0.304370	0.000
O...O	22764.300	0.149000	27.879
Si...O	1283.91	0.32052	10.66
Ge...O	1497.3996	0.325646	16.000
(b) Species	<i>Y</i> (e)	<i>K</i> /eV \AA^{-2}	
La	3.00 ^a , -0.25 ^b	Rigid ion ^a , 145.0 ^b	
O	-2.89 ^a , -2.86 ^b	74.92	
Si	4.00	Rigid ion	
Ge	4.00	Rigid ion	

^a Ge-apatites. ^b Si-apatites.

Table 2 Parameters for the O–H interaction: (a) intramolecular Morse potential and (b) intermolecular Buckingham potential

(a) Intramolecular interaction	<i>D</i> /eV	$\beta/\text{\AA}^{-1}$	<i>r_s</i> / \AA
O–H	7.0525	2.1986	0.9485
(b) Intermolecular interaction	<i>A</i> /eV	$\rho/\text{\AA}$	<i>C</i> /eV \AA^6
O–H	311.97	0.25	0.00

are based on the Born model for polar solids where the interactions between ions are represented in terms of a long-range Coulombic term plus an analytical function representing short-range repulsive and van der Waals interactions. For this study, the short range interactions were modelled using the Buckingham potential:

$$V_{ij}(r) = A_{ij}\exp(-r/\rho_{ij}) - C_{ij}/r^6 \quad (1)$$

where *r* is the interatomic distance and *A*, ρ and *C* are empirically derived parameters. Charged defects will polarise nearby ions in the lattice and therefore, accurate calculation of defects energies requires the inclusion of electronic polarisability in the model, which is incorporated *via* the shell model.³⁸ Point defects were modelled using the Mott-Littleton approach, in which a defect is introduced into the energy minimised lattice, and the surrounding ions partitioned into two regions.^{34,39} An inner sphere of ions immediately surrounding the point defect (region 1) is then relaxed explicitly whilst the crystal bulk (region 2) is treated by computationally less expensive quasi-continuum methods. Table 1 lists the interatomic potentials used for the silicate and germanate systems, transferred from recent atomistic modelling work on apatites.^{9,13-15}

As with previous modelling studies on protons in perovskite oxides³² and silicate minerals⁴⁰ the OH interaction was treated using an attractive Morse potential (with Coulomb subtraction):

$$V(r) = D\{1 - \exp[-\beta(r - r_0)]\}^2 \quad (2)$$

using parameters (listed in Table 2) developed from *ab initio* quantum mechanical cluster calculations,⁴¹ with a point charge

representation of the surrounding lattice. The dipole moment of the OH group was simulated by placing charges of -1.4263 and $+0.4263$ on the O and H species, respectively (overall charge -1.00) in accordance with this study. Additional Buckingham parameters were employed to simulate the interaction of the lattice oxygen atoms with the hydroxyl unit.^{32,40}

3 Results and discussion

3.1 Structural modelling and oxygen interstitials

The starting point for our study is the modelling of the crystal structures and comparison with experiment for the six different apatite systems: two stoichiometric ($\text{La}_8\text{Ba}_2(\text{Si}/\text{GeO}_4)_6\text{O}_2$), two cation deficient ($\text{La}_{9.33}(\text{Si}/\text{GeO}_4)_6\text{O}_2$) and two oxygen excess ($\text{La}_{9.67}(\text{Si}/\text{GeO}_4)_6\text{O}_{2.5}$). The structure of apatite materials (shown in Fig. 1) can be described as comprising isolated Si/GeO_4 tetrahedra that are arranged so as to form distinct oxide-ion and La channels running parallel to the c -axis.

For the stoichiometric $\text{La}_8\text{Ba}_2(\text{Si}/\text{GeO}_4)_6\text{O}_2$ systems, $P63/m$ symmetry was adopted, following the structure reported earlier.^{11,13} In order for the incorporation of cation vacancies or oxygen excess without the use of fractional occupancies, supercells with $P1$ symmetry were employed for $\text{La}_{9.33}(\text{Si}/\text{GeO}_4)_6\text{O}_2$ ($1 \times 1 \times 3$ supercell, two La vacancies) and $\text{La}_{9.67}(\text{Si}/\text{GeO}_4)_6\text{O}_{2.5}$ ($2 \times 1 \times 3$ supercell, two La vacancies and three oxygen interstitials) to match the experimental compositions. Following on from previous experimental and simulation work,^{9–15} the La vacancy defects favour the La2 ($1/3, 2/3, z$) position. The oxygen interstitial positions for the excess systems were in the corresponding sites of the experimental structures of León-Reina *et al.*¹⁷

Simulations of the crystal structures then involve energy minimisation calculations allowing the unit cell parameters and ion positions to relax. The calculated and experimental lattice parameters for all six systems are compared in Table 3. Good agreement is shown between the experimental and simulated structures, even for the more complex non-stoichiometric Ge-apatites such as $\text{La}_{9.67}(\text{GeO}_4)_6\text{O}_{2.5}$; this system in particular has not been as widely studied as the Si-apatites by simulation techniques. This degree of agreement provides support for the validity of the interatomic potentials used for these materials. It should be stressed that the complex apatite structures make it non-trivial to successfully reproduce the experimental structures

on this scale. The differences in unit cell parameters are nearly all less than 0.15 \AA and in most cases much less. The bond lengths are also found to reproduce the experimental values to within 2–3%. These optimised structures have then been used for subsequent defect and water incorporation calculations.

The importance of oxygen interstitials for ion conduction in apatite materials has been well established. It is also well known that the lack of interstitial oxide ions means that the fully stoichiometric apatite systems have much lower ionic conductivities and higher activation energies compared to their non-stoichiometric counterparts. As the higher conductivity has been attributed to the presence of mobile oxygen interstitials, an extensive study of the local structure around the oxygen interstitials for all the six systems described above is presented. For the Ge-based systems in particular, the defects have not been modelled as widely as for the silicate-based systems.

From detailed defect calculations, the most stable oxygen interstitial sites are found to lie at the periphery of the La1/O4 channel for the silicate systems, which is shown in Fig. 2 for the representative system $\text{La}_{9.67}(\text{SiO}_4)_6\text{O}_{2.5}$. For the Ge based systems, the interstitial position could either be classed as at the channel periphery (as for the silicates), or in between two GeO_4 units in adjacent channels, since both give identical relaxed configurations, illustrated in Fig. 3 for the representative germanate $\text{La}_{9.67}(\text{GeO}_4)_6\text{O}_{2.5}$. Interestingly, the combined study of Si-based and Ge-based apatites highlights, that while the Si-based systems results in the formation of a pseudo “ SiO_5 ” unit,¹⁵ the Ge-based systems tend to form a pseudo “ Ge_2O_9 ”,¹⁴ which is

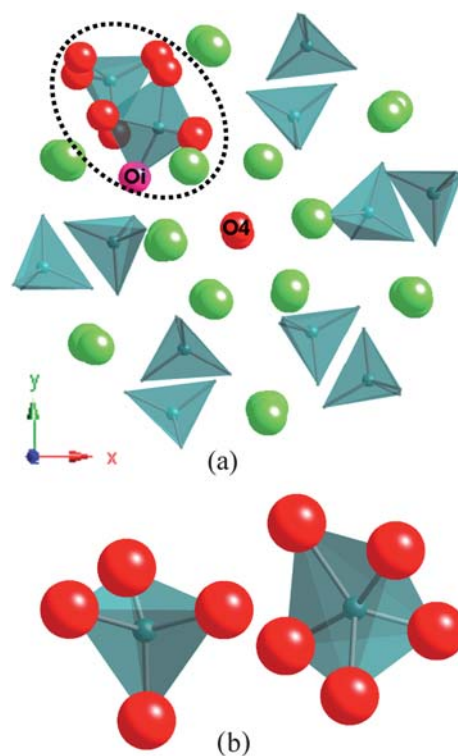


Fig. 2 $\text{La}_{9.67}(\text{SiO}_4)_6\text{O}_{2.5}$ structure showing the position of the oxygen interstitial (a) initial configuration at channel periphery; Oi is the oxygen interstitial, and O4 is the channel oxygen along the c -axis (b) final relaxed local structure showing the “ SiO_5 ” unit.

Table 3 Comparison of structural parameters for stoichiometric ($\text{La}_8\text{Ba}_2(\text{Si}/\text{GeO}_4)_6\text{O}_2$), La-deficient ($\text{La}_{9.33}(\text{Si}/\text{GeO}_4)_6\text{O}_2$) and oxygen excess ($\text{La}_{9.67}(\text{Si}/\text{GeO}_4)_6\text{O}_{2.5}$) apatite systems

System		$a/\text{\AA}$	$b/\text{\AA}$	$c/\text{\AA}$
$\text{La}_8\text{Ba}_2(\text{SiO}_4)_6\text{O}_2$	Expt. ¹¹	9.7776(2)	9.7776(2)	7.3223(1)
	Calc.	9.8685	9.8685	7.2492
$\text{La}_{9.33}(\text{SiO}_4)_6\text{O}_2$	Expt. ¹¹	9.7248(1)	9.7248(1)	7.1895(1)
	Calc.	9.7911	9.7911	7.0767
$\text{La}_{9.67}(\text{SiO}_4)_6\text{O}_{2.5}$	Expt. ¹⁷	9.7256(1)	9.7256(1)	7.1863(1)
	Calc.	9.7909	9.7909	7.0971
$\text{La}_8\text{Ba}_2(\text{GeO}_4)_6\text{O}_2$	Expt. ²⁶	9.9768(3)	9.9768(3)	7.4039(2)
	Calc.	10.1004	10.1004	7.2549
$\text{La}_{9.33}(\text{GeO}_4)_6\text{O}_2$	Expt. ⁴²	9.9117(1)	9.9117(1)	7.2833(1)
	Calc.	10.0295	10.0020	7.1057
$\text{La}_{9.67}(\text{GeO}_4)_6\text{O}_{2.5}$	Expt. ¹⁶	9.9374(1)	9.9374(1)	7.2835(1)
	Calc.	10.0850	10.0311	7.0943

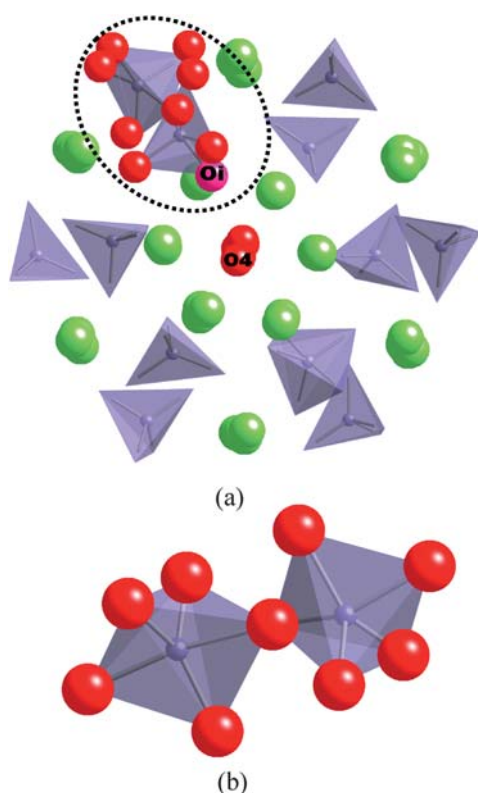


Fig. 3 $\text{La}_{9.67}(\text{GeO}_4)_6\text{O}_{2.5}$ structure showing the position of the oxygen interstitial (a) initial configuration of neighbouring GeO_4 tetrahedra; O_i is the oxygen interstitial, and O_4 is the channel oxygen along the c -axis (b) final relaxed local structure showing the “ Ge_2O_9 ” unit.

confirmed here. In both cases considerable relaxation of nearby tetrahedral units is found.

The calculated interstitial site at the channel periphery has been supported by neutron diffraction studies of oxygen excess $\text{La}_{9.33+x}(\text{Si/GeO}_4)_6\text{O}_{2+3x/2}$ ^{13,16,17,27,28} and by ²⁹Si NMR and Raman studies of a range of alkaline-earth doped and Ti doped apatite silicates.¹² A similar periphery interstitial site is found in a recent study by Ali *et al.*²³ of the Mg-doped silicate $\text{La}_{9.71}(\text{Si}_{5.81}\text{Mg}_{0.19})\text{O}_{26.37}$ using Rietveld refinement and the maximum-entropy method (MEM) of synchrotron X-ray diffraction data.

We note however that other recent studies^{19,20} find interstitial sites that do not lie at the very periphery of the channel, but more inside the channel, and Savignat *et al.*²⁰ also suggest that the channel oxide ions are involved in the conduction process. These experimental reports of different interstitial sites highlight the complexity of these apatite materials, which are non-trivial to study by diffraction techniques, since such techniques only give the average structure, whereas the modelling studies have highlighted considerable localised distortions. It is also possible that the interstitial site in the apatite silicates may depend on synthesis conditions and thermal history, which warrants further detailed structural studies of samples prepared under different heating regimes.

Nevertheless, other experimental support for the importance of the SiO_4 substructure in the conduction process, and hence for the conclusions from the modelling work, include:

i. The observation of significant conduction perpendicular to the channels from single crystal studies of Nakayama *et al.*,²⁴ which has been suggested as being due to “SN2”-type exchange processes.¹³

ii. ¹⁸O/¹⁶O exchange measurements by Kharlamova *et al.*,²⁵ which showed very high levels of exchange, indicating that the Si–O oxygen atoms are exchangeable.

For the germanate systems, the interstitial effectively creates a “ Ge_2O_9 ” unit leading to significant local structural distortions illustrated in Fig. 3. This is similar to the results from recent structural and modelling studies, where an interstitial site between two GeO_4 tetrahedra has been proposed.^{14,27,28} For example, the presence of five-coordinate Ge has recently been proposed from neutron diffraction studies by Pramana *et al.*²⁷ on the oxygen-excess apatite $\text{La}_{10}(\text{GeO}_4)_6\text{O}_3$. Indeed, for the germanates, there is general consensus in the neutron diffraction studies from different groups.^{16,27,28}

In general, the simulation results indicate that the effect of interstitial ions on the local structure of Si- and Ge-apatites needs to be considered; this is not straightforward when using average structural techniques, but is related to the high thermal displacement parameters of the tetrahedra oxide ions that are observed in diffraction studies.

3.2 Water incorporation: local structure of protonic defect

The enhanced ionic conductivity observed by León-Reina *et al.*²² for $\text{La}_{10-x}(\text{GeO}_4)_6\text{O}_{3-1.5x}$ materials in wet atmospheres has been attributed to proton conduction below 600 K. Furthermore, Orera and Slater²⁶ have investigated the ability to incorporate water in a range of Si/Ge-apatites including $\text{La}_{9.33}(\text{SiO}_4)_6\text{O}_2$ and $\text{La}_8\text{Ba}_2(\text{GeO}_4)_6\text{O}_2$; they have suggested that water incorporation leads to the incorporation of interstitial oxide ions in addition to protons, and their recent studies showed no clear isotope effect between H_2O and D_2O measurements suggesting the enhancement may be related to enhanced oxide ion conduction. It is therefore clear that the effect of water incorporation warrants further investigation.

In order to examine the mechanism of water incorporation, it is important first to determine the most favoured protonic site within the lattice for the different apatite-based systems. It is known that hydrogen is not located directly from X-ray diffraction due to the insensitivity of X-rays towards light elements. Evidence of which site the protonic defect prefers in Si- or Ge-apatites has not been reported thus far.

Here, the protonic defect is treated as a hydroxyl group since the proton is associated with an oxygen ion. Following our previous work on protons in perovskite-type oxides,³² the simulation techniques can be used to determine the most energetically favourable site. To do this, an isolated hydroxyl group was placed on each of the lattice oxygen sites with the proton allowed to orient in different directions, and full relaxation around these species. The resulting OH defect energies for all oxygen sites are listed in Table 4.

These defect energies clearly show that the lowest energy OH site is along the O_4 channel for all the apatites considered; in comparison to the other lattice oxygen sites, this O_4 channel site is favoured by over 2 eV. The lowest energy configuration is illustrated in Fig. 4, using $\text{La}_{9.67}(\text{Si/GeO}_4)_6\text{O}_{2.5}$ as representative

Table 4 Isolated energies E_{OH} of the proton positions (OH_{O}) at different lattice oxygen sites

System	Energies E_{OH}/eV				
	O1 ^a	O2 ^a	O3 ^a	O4 ^b	O5 ^c
$\text{La}_8\text{Ba}_2(\text{SiO}_4)_6\text{O}_2$	10.24	9.50	8.86	5.95	—
$\text{La}_{9.33}(\text{SiO}_4)_6\text{O}_2$	10.31	10.80	9.35	6.26	—
$\text{La}_{9.67}(\text{SiO}_4)_6\text{O}_{2.5}$	9.85	8.52	8.45	6.02	8.29
$\text{La}_8\text{Ba}_2(\text{GeO}_4)_6\text{O}_2$	9.75	9.22	8.50	5.50	—
$\text{La}_{9.33}(\text{GeO}_4)_6\text{O}_2$	9.85	9.68	8.41	5.42	—
$\text{La}_{9.67}(\text{GeO}_4)_6\text{O}_{2.5}$	9.51	8.12	7.80	5.75	8.22

^a Tetrahedra oxygen atoms. ^b Channel O4 (labelled O5 in some papers).^{8–13}

^c Intrinsic lattice interstitials present in the oxygen excess systems only.

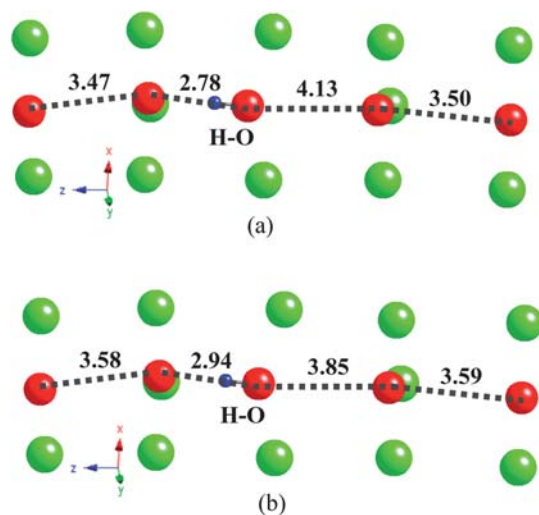


Fig. 4 Most favourable O–H site (in blue) within the apatite lattice identified along the c -axis O4 channel with the final O4–O4 interatomic separations indicated in Å; (a) $\text{La}_{9.67}(\text{SiO}_4)_6\text{O}_{2.5}$ and (b) $\text{La}_{9.67}(\text{GeO}_4)_6\text{O}_{2.5}$ (O4 oxygen in red; La1 lanthanum in green).

systems, where the orientation of the H along the O4 channel is highlighted. Although there is no direct comparison, this arrangement agrees well with the naturally occurring hydroxy-apatites (e.g. $\text{Ca}_{10}(\text{PO}_4)_6(\text{OH})_2$), in which the hydroxyl ions lie along the oxide channels with distances of about 2.4 Å from one O–H to another.^{43–46} Our results suggest a localised displacement of the O–H defect towards one of the neighbouring O4 oxygen atoms, with a longer inter-atomic separation to the other O4 ion. As shown in Fig. 4, the proton is the most stable when pointing towards a neighbouring O4 ion in the channel.

The final relaxed interatomic separations along the O4 oxygen channel for all six systems are listed in Table 5. The relaxed geometry gives typical O–H bond lengths of approximately 0.99 Å. The inter-atomic (O–H)–O4 distances are also derived, where the typical hydrogen bonding distances are between 1.6–2.0 Å. Finally the O4–(O–H) distances are calculated, where a decrease in the neighbouring O4–O4 distance is noted from approximately 3.5–3.6 Å (dry) to 2.8–2.9 Å (hydrated). The O4–O4 distances further away from the defect remain about 3.5–3.6 Å, similar to the O4–O4 distances in the dry samples. However, a notable increase of the H–O4–O4 distance to about 3.85–4.1 Å is calculated and shown in Fig. 4. These large shifts in

Table 5 Local interatomic distances for the most favoured OH position, along the c -axis oxide channel (shown in Fig. 4)

System	O–H (intra)/Å	(O)H–O4/Å	(H)O–O4/Å	O4–O4/Å
		Hydrated	Hydrated	Dry
$\text{La}_8\text{Ba}_2(\text{SiO}_4)_6\text{O}_2$	0.98	2.78	4.06	3.66
$\text{La}_{9.33}(\text{SiO}_4)_6\text{O}_2$	0.99	2.75	3.97	3.56
$\text{La}_{9.67}(\text{SiO}_4)_6\text{O}_{2.5}$	0.99	2.78	4.13	3.57
$\text{La}_8\text{Ba}_2(\text{GeO}_4)_6\text{O}_2$	0.99	2.81	4.08	3.70
$\text{La}_{9.33}(\text{GeO}_4)_6\text{O}_2$	0.99	2.62	3.91	3.64
$\text{La}_{9.67}(\text{GeO}_4)_6\text{O}_{2.5}$	0.99	2.94	3.85	3.62

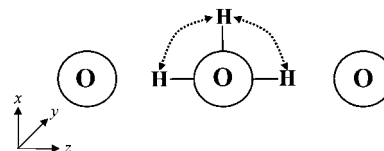


Fig. 5 Schematic showing rotation of the OH group in the xz plane.

O4 positions due to proton incorporation may explain the experimental observation for some compositions^{19,20} of interstitial oxygen positions close to the channel centre, and highlights the need for further neutron diffraction studies comparing samples treated in dry and wet atmospheres.

Any proton conduction down the O4 channel will require OH rotation before proton transfer. We have therefore carried out preliminary calculations on possible rotation barrier configurations, shown in Fig. 5. The relative defect energies when the hydrogen is oriented away from the channel (in xz and yz planes) are 1.5 eV higher than when the hydroxyl group is along the channel (perpendicular to the c -axis). This high rotational barrier suggests that proton conduction through rotation and hopping down the O4 channel is unfavourable. This topic warrants further investigation and is currently being examined by DFT-based methods.

3.3 Water incorporation: reaction mechanisms

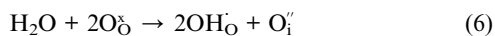
For acceptor-doped perovskite systems (such as Y-doped BaZrO_3 or BaCeO_3) water incorporation occurs at the oxide ion vacancies,^{30–32} which lead to the presence of proton defects (hydroxyl ions) according to the following reaction:



For these perovskite proton conductors, the key defects are oxide ion vacancies. Therefore as well as incorporating protons, this reaction leads to the filling of oxide ion vacancies, hence lowering the oxide ion conduction. In contrast, the key defects for the apatite-type materials are oxygen interstitials, and so in this case water incorporation could also lead to the creation of more interstitial oxide ions. Therefore, the process for water incorporation in Si- or Ge-apatites is less clear since they do not contain a high level of oxygen vacancies.

In order to assess the enhanced conductivity reported in wet atmospheres,²² Orera *et al.*²⁶ proposed three relevant defect equations for water incorporation, according to whether the

proton favours an interstitial oxide ion (O_i'') or the conventional lattice oxide ion site (O_{δ}):



where eqn (4) involves a hydroxyl on the conventional lattice site (OH_O) and one hydroxyl interstitial (OH_i); eqn (5) involves reaction with an oxygen interstitial site resulting in hydroxyl interstitials; eqn (6), involves a hydroxyl ion on the conventional lattice site and the formation of an “additional” oxygen interstitial. We should stress that for oxygen stoichiometric samples, where there are nominally no interstitial oxide ions, eqn (4) and (6) will apply, while for samples containing oxygen excess, eqn (5) and (6) are relevant.

The magnitude of the water incorporation (hydration) energy (E_{H_2O}) varies with oxide systems, and indicates the extent of protonation at a given temperature. However, analyses of the thermodynamics of protonic defects in apatites have been limited. Here the same successful methodology as used previously for evaluating the energetics of water incorporation (E_{H_2O}) in proton-conducting perovskites³² was employed for the eqn (4), (5) and (6) using the following eqn (7), (8) and (9) respectively:

$$E_{H_2O} = E(OH_O) + E(OH_i) + E_{PT} \quad (7)$$

$$E_{H_2O} = 2E(OH_i) - E(O_i'') + E_{PT} \quad (8)$$

$$E_{H_2O} = 2E(OH_O) + E(O_i'') + E_{PT} \quad (9)$$

where $E(OH_O)$ is the energy associated with substitution of a lattice oxygen with an OH^- group, $E(OH_i)$ is the energy associated with replacing an oxygen interstitial with a hydroxy group, $E(O_i'')$ is the energy associated with the introduction of an oxygen interstitial and E_{PT} is the energy (-11.77 eV) of the gas phase proton transfer reaction, $O^{2-} + H_2O \rightarrow 2OH^-$, as employed previously.^{32,41}

The total water incorporation energies are listed in Table 6 for all six systems. The $E(OH_O)$ term used was the favoured hydroxyl site along the O4 channel, and the lowest oxygen interstitial position was used to calculate the $E(OH_i)$ term.

The results in Table 6 reveal three key points. First, the germanate-based apatites have the most favourable water incorporation energies, indicating greater affinity for water. These results

Table 6 Water incorporation energies (E_{H_2O}) for the relevant defect reactions

System	E_{H_2O}/eV		
	Eqn (4)	Eqn (5)	Eqn (6)
$\text{La}_8\text{Ba}_2(\text{SiO}_4)_6\text{O}_2$	0.29	—	0.35
$\text{La}_{9.33}(\text{SiO}_4)_6\text{O}_2$	0.27	—	0.81
$\text{La}_{9.67}(\text{SiO}_4)_6\text{O}_{2.5}$	—	1.79	0.00
$\text{La}_8\text{Ba}_2(\text{GeO}_4)_6\text{O}_2$	-0.73	—	-1.52
$\text{La}_{9.33}(\text{GeO}_4)_6\text{O}_2$	-1.29	—	-2.11
$\text{La}_{9.67}(\text{GeO}_4)_6\text{O}_{2.5}$	—	1.51	-1.76

accord well with the experimental studies,^{22,26} which show higher water incorporation levels in Ge-apatites at intermediate temperatures in wet atmospheres.

Second, an important finding is that eqn (6) is the most favourable water incorporation mechanism in the Ge-apatites, which involves the formation of “additional” oxygen interstitial ions. These results therefore suggest that the reported enhancement in ionic conductivity for Ge-based apatites in wet atmospheres²² may be related to increased oxide-ion conduction. This is also consistent with recent studies²⁶ showing no clear isotope effect between H_2O and D_2O measurements indicating no significant proton conductivity.

Finally, even though there are currently no experimental values on these apatites for direct comparison, the magnitudes of E_{H_2O} are highly comparable with those measured for proton incorporation in perovskite materials; for example, values of between about -0.8 and -1.7 eV are found for systems such as doped BaCeO_3 and doped BaZrO_3 .^{30,47} The exothermic values indicate that the dissolution of protons is favoured by decreasing temperatures.

4 Conclusion

Advanced modelling techniques have been used to provide atomic-scale insights into the local defect structures and water incorporation mechanisms in six apatite ionic conductors: two stoichiometric ($\text{La}_8\text{Ba}_2(\text{Si}/\text{GeO}_4)_6\text{O}_2$), two cation deficient ($\text{La}_{9.33}(\text{Si}/\text{GeO}_4)_6\text{O}_2$) and two oxygen excess ($\text{La}_{9.67}(\text{Si}/\text{GeO}_4)_6\text{O}_{2.5}$) materials. The following main points emerge:

1) The observed complex structures of all six apatite materials have been reproduced successfully by the simulation methods. As with previous investigations, an extensive modelling study of the local defect structure identifies the prime oxygen interstitial location as neighbouring the Si/GeO_4 tetrahedra in accord with neutron diffraction and ^{29}Si NMR data. The simulation results on interstitial defects indicate significant local structural distortions around the Si and Ge atoms, which are difficult to probe by average structural techniques.

2) The local OH site is found to be along the O4 channel with the proton pointing towards a neighbouring O4 oxygen. This is in agreement with the structures of naturally occurring hydroxy-apatites, in which the hydroxyl ions lie along the oxide channel.

3) The water incorporation (hydration) energies agree well with experiment, in that the germanate-based apatites allow significantly higher water contents. In addition, the exothermic energies for the favoured reaction mechanism for water incorporation suggests the formation of “additional” oxygen interstitial ions for germanate systems in wet atmospheres. This may account for the reported enhancements of ionic conductivity rather than proton conduction, but warrants further investigation.

Acknowledgements

The authors would like to acknowledge the EPSRC (Grant EP/F013248/1), and the HECToR supercomputer facilities within the Materials Chemistry Consortium (Grant EP/F067496/1).

References

- 1 B. C. H Steele and A. Heinzel, *Nature*, 2001, **414**, 345.
- 2 R. M. Ormerod, *Chem. Soc. Rev.*, 2003, **32**, 17.
- 3 A. Atkinson, S. Barnett, R. J. Gorte, J. T. S. Irvine, A. J. McEvoy, M. Mogensen and S. C. Singhal, *Nat. Mater.*, 2004, **3**, 17.
- 4 Z. P. Zhou and S. M. Haile, *Nature*, 2004, **431**, 170.
- 5 (a) S. Nakayama, H. Aono and Y. Sadaoka, *Chem. Lett.*, 1995, 431; (b) S. Nakayama, T. Kagayama, H. Aono and Y. Sadaoka, *J. Mater. Chem.*, 1995, **5**, 1801; (c) S. Nakayama, Y. Higuchi, Y. Kondo and M. Sakamoto, *Solid State Ionics*, 2004, **170**, 219.
- 6 S. Tao and J. T. S. Irvine, *Mater. Res. Bull.*, 2001, **36**, 1245.
- 7 (a) H. Yoshioka and S. Tanase, *Solid State Ionics*, 2005, **176**, 2395; (b) Y. Masubachi, M. Higuchi, T. Takeda and S. Kikkawa, *Solid State Ionics*, 2006, **177**, 263.
- 8 J. E. H. Sansom, D. Richings and P. R. Slater, *Solid State Ionics*, 2001, **139**, 205.
- 9 (a) J. R. Tolchard, M. S. Islam and P. R. Slater, *J. Mater. Chem.*, 2003, **13**, 1956; (b) J. R. Tolchard, P. R. Slater and M. S. Islam, *Adv. Funct. Mater.*, 2007, **17**, 2564.
- 10 (a) J. E. H. Sansom, J. R. Tolchard, P. R. Slater and M. S. Islam, *Solid State Ionics*, 2004, **167**, 17; (b) A. Najib, J. E. H. Sansom, J. R. Tolchard, P. R. Slater and M. S. Islam, *Dalton Trans.*, 2004, 3106; (c) A. Al-Yasari, A. Jones, A. Orera, D. C. Apperley, D. Driscoll, M. S. Islam and P. R. Slater, *J. Mater. Chem.*, 2009, **19**, 5003.
- 11 (a) J. E. H. Sansom, A. Najib and P. R. Slater, *Solid State Ionics*, 2004, **175**, 353; (b) J. R. Tolchard, J. E. H. Sansom, M. S. Islam and P. R. Slater, *Dalton Trans.*, 2005, 1273.
- 12 (a) J. E. H. Sansom, J. R. Tolchard, M. S. Islam, D. Apperley and P. R. Slater, *J. Mater. Chem.*, 2006, **16**, 1410; (b) A. Orera, D. Headspith, D. C. Apperley, M. G. Francesconi and P. R. Slater, *J. Solid State Chem.*, 2009, **182**, 3294; (c) A. Orera, E. Kendrick, D. C. Apperley, V. M. Orera and P. R. Slater, *Dalton Trans.*, 2008, 5296.
- 13 (a) E. Kendrick, M. S. Islam and P. R. Slater, *J. Mater. Chem.*, 2007, **17**, 3104; (b) E. Kendrick, J. R. Tolchard, J. E. H. Sansom, M. S. Islam and P. R. Slater, *Faraday Discuss.*, 2007, **134**, 181.
- 14 E. Kendrick, M. S. Islam and P. R. Slater, *Chem. Commun.*, 2008, 715.
- 15 A. Jones, P. R. Slater and M. S. Islam, *Chem. Mater.*, 2008, **20**, 5055.
- 16 (a) L. León-Reina, M. C. Martín-Sedeño, E. R. Losilla, A. Cabeza, M. Martínez-Lara, S. Bruque, F. M. B. Marques, D. V. Sheptyakov and M. A. G. Aranda, *Chem. Mater.*, 2003, **15**, 2099; (b) L. León-Reina, E. R. Losilla, M. Martínez-Lara, S. Bruque, A. Llobet, D. V. Sheptyakov and M. A. G. Aranda, *J. Mater. Chem.*, 2005, **15**, 2489.
- 17 L. León-Reina, E. R. Losilla, M. Martínez-Lara, S. Bruque and M. A. G. Aranda, *J. Mater. Chem.*, 2004, **14**, 1142.
- 18 (a) A. L. Shaula, V. V. Kharton and F. M. B. Marques, *J. Solid State Chem.*, 2005, **178**, 2050; (b) Y. V. Pivak, V. V. Kharton, A. A. Yaremchenko, S. O. Yakovlev, A. V. Kovalevsky, J. R. Frade and F. M. B. Marques, *J. Eur. Ceram. Soc.*, 2007, **27**, 2445.
- 19 E. Bechade, O. Masson, T. Iwata, I. Julien, K. Fukuda, P. Thomas and E. Champion, *Chem. Mater.*, 2009, **21**, 2508.
- 20 (a) S. Guillot, S. B-Savignat, S. Lambert, R.-N. Vannier, P. Roussel and F. Porcher, *J. Solid State Chem.*, 2009, **182**, 3358; (b) S. B-Savignat, A. Vincent, S. Lambert and F. Gervais, *J. Mater. Chem.*, 2007, **17**, 2078.
- 21 (a) Q. H. Shi, J. F. Wang, J. P. Zhang, J. Fan and G. D. Stucky, *Adv. Mater.*, 2006, **18**, 1038; (b) J. H. Zhan, Y. H. Tseng, J. C. C. Chan and C. Y. Mou, *Adv. Funct. Mater.*, 2005, **15**, 2005; (c) G. He, T. Dahl, A. Veis and A. George, *Nat. Mater.*, 2003, **2**, 552.
- 22 L. León-Reina, J. M. Porras-Vasquez, E. R. Losilla and M. A. G. Aranda, *J. Solid State Chem.*, 2007, **180**, 1250.
- 23 (a) R. Ali, M. Yashima, Y. Matshita, H. Yoshioka and F. Izumi, *J. Solid State Chem.*, 2009, **182**, 2846; (b) R. Ali, M. Yashima, Y. Matshita, H. Yoshioka, K. Ohoyama and F. Izumi, *Chem. Mater.*, 2008, **20**, 5203.
- 24 S. Nakayama, M. Sakamoto, M. Higuchi and K. Kodaira, *J. Mater. Sci. Lett.*, 2000, **19**, 91.
- 25 T. Kharlamova, S. Pavlova, V. Sadykov, T. Krieger, L. Batuev, V. Muzykantov, N. Uranov and Chr. Argiris, *Solid State Ionics*, 2009, **180**, 796.
- 26 A. Orera and P. R. Slater, *Solid State Ionics*, 2009, DOI: 10.1016/j.ssi.2008.12.014.
- 27 (a) S. S. Pramana, W. T. Klooster and T. J. White, *Acta Crystallogr., Sect. B: Struct. Sci.*, 2007, **63**, 597; (b) S. S. Pramana, W. T. Klooster and T. J. White, *J. Solid State Chem.*, 2008, **181**, 1717.
- 28 E. Kendrick, A. Orera and P. R. Slater, *J. Mater. Chem.*, 2009, **19**, 7955.
- 29 J. B. Goodenough, *Annu. Rev. Mater. Res.*, 2003, **33**, 91.
- 30 K. D. Kreuer, *Annu. Rev. Mater. Res.*, 2003, **33**, 333.
- 31 H. Iwahara, *Solid State Ionics*, 1996, **86-9**, 9.
- 32 (a) R. A. Davies, M. S. Islam and J. D. Gale, *Solid State Ionics*, 1999, **126**, 323; (b) M. S. Islam, *J. Mater. Chem.*, 2000, **10**, 1027; (c) G. C. Mather and M. S. Islam, *Chem. Mater.*, 2005, **17**, 1736; (d) C. A. J. Fisher and M. S. Islam, *Solid State Ionics*, 1999, **118**, 355.
- 33 E. Kendrick, M. Russ and P. R. Slater, *Solid State Ionics*, 2008, **179**, 819.
- 34 J. D. Gale, *J. Chem. Soc., Faraday Trans.*, 1997, **93**, 629.
- 35 C. R. A. Catlow, *Solid State Chemistry-Techniques*, Clarendon Press, Oxford, 1987.
- 36 C. R. A. Catlow, *Computer Modelling in Inorganic Crystallography*, Academic Press, San Diego, 1997, p. 340.
- 37 F. M. Higgins, N. H. de Leeuw and S. C. Parker, *J. Mater. Chem.*, 2002, **12**, 124; (a) D. W. Lewis, C. R. A. Catlow and J. M. Thomas, *Faraday Discuss.*, 1997, **106**, 451.
- 38 B. Dick and A. Overhauser, *Phys. Rev.*, 1958, **112**, 90.
- 39 N. F. Mott and M. J. Littleton, *Trans. Faraday Soc.*, 1938, **34**, 485.
- 40 (a) K. Wright and C. R. A. Catlow, *Phys. Chem. Miner.*, 1994, **20**, 515; (b) A. Gatzemeier and K. Wright, *Phys. Chem. Miner.*, 2006, **33**, 115.
- 41 P. Saul and C. R. A. Catlow, *Philos. Mag. B*, 1985, **51**, 107.
- 42 P. Berastegui, S. Hull, F. J. Garcia-Garcia and J. Grins, *J. Solid State Chem.*, 2002, **168**, 294.
- 43 D. Zahn and O. Hochrein, *J. Solid State Chem.*, 2008, **181**, 1712.
- 44 N. H. de Leeuw, *Phys. Chem. Chem. Phys.*, 2002, **4**, 3865.
- 45 A. S. Posner, A. Perloff and A. F. Diorio, *Acta Crystallogr.*, 1958, **11**, 308.
- 46 M. I. Kay, R. A. Young and A. S. Posner, *Nature*, 1964, **204**, 1050.
- 47 T. Norby and Y. Larring, *Curr. Opin. Solid State Mater. Sci.*, 1997, **2**, 593.